^{57}Fe Mössbauer Study of the Electrochemical Reaction of Lithium with Triclinic Iron Vanadate

S. Denis,*,† R. Dedryvère,‡ E. Baudrin,† S. Laruelle,† M. Touboul,†
J. Olivier-Fourcade,‡ J. C. Jumas,‡ and J. M. Tarascon†

Laboratoire de Réactivité et de Chimie des Solides, UPRES A 6007, 33 rue Saint-Leu, 80039 Amiens Cedex, France, and Laboratoire des Agrégats Moléculaires et des Matériaux Inorganiques (UMR 5072), Université Montpellier II, CC15, Place Eugène Bataillon, 34095 Montpellier Cedex 5, France

Received May 12, 2000. Revised Manuscript Received September 19, 2000

The electrochemical reaction of lithium with triclinic $FeVO_4$ (a = 6.714(1) Å, b = 8.060(2) Å, c = 9.352(2) Å, α = 96.678(1)°, β = 106.641(1)°, and γ = 101.523(1)°, P-1) has been investigated by means of ^{57}Fe Mössbauer spectroscopy in order to complement the previous X-ray diffraction and X-ray absorption near edge structure studies on the same system. A complex $Fe^{III} \rightarrow Fe^{II} \rightarrow Fe^0$ or $Fe^{III} \rightarrow Fe^{II}$, Fe^0 reduction process has been detected upon the first discharge of the battery down to 0.02 V, with in addition the iron reoxidation during the next charge step. A mechanism based on "lithium adsorption" is proposed in order to explain this unexpected behavior.

1. Introduction

With the great economic ascent of the portable market, an intense research activity has been generated toward the development of improved batteries. A suitable battery for these kinds of electronic devices (laptop computers, cell phones, etc.) requires several parameters such as its miniaturization, high performance, long shelf life, and also its safety. Li-metal batteries display the best performances in terms of mass and volumic energy densities. However, because of safety problems, the concept of Li-ion batteries was developed over these last years.

In the Li-ion technology, both electrodes are intercalation materials. Typically, graphite serves as the anode and lithiated transition metal oxide serves as the cathode. In view of increasing the capacity of such batteries, current research is mainly shared between two activities: (i) improving the existing lithiated Co-, Ni-, or Mn-based oxides or searching for new ones; (ii) searching for alternatives to the graphite negative electrode.

In the second area, an intense effort has been put into research in order to get novel negative electrode materials with a large capacity and a strong reducing power. This is why several different types of anode materials have been studied these past years such as, for example, lithium alloys,[1,2] carbonaceous materials,[3−5] nitrides,[6−9] sulfides,[10−12] and metal oxides.[13,14] Among them are vanadates which have recently attracted potential interest as negative electrode materials in rechargeable Li-ion batteries since some of them can react with large amounts of lithium at a low mean voltage (leading to specific capacities of about 800−900 mA h g^{-1}).[15]

However, the reaction mechanism of these materials with lithium is not completely understood yet. Previous X-ray diffraction (XRD) and X-ray absorption near edge structure (XANES) investigations performed on the Li_x-$FeVO_4$/Li system gave some insight in the understanding of the Li uptake/removal process.[16] The main results demonstrated the occurrence of several new phases during the first reduction of the cell followed by a progressive amorphization of the lithiated product. Finally, a material with delocalized electronic states around the vanadium and iron sites has been determined at the end of the discharge at 0.02 V vs Li. On

† Laboratoire de Réactivité et de Chimie des Solides, UPRES A 6007.
‡ Laboratoire des Agrégats Moléculaires et des Matériaux Inorganiques (UMR 5072), Université Montpellier II.

(1) Idota, Y.; Kubota, T.; Matsufuji, A.; Maekawa, Y.; Miyasaka, T. *Science* **1997**, *276*, 1395.
(2) Idota, Y.; Mishima, M.; Miyaki, Y.; Kubota, T.; Miyasaka, T. US Patent 5,618,640, 1997.
(3) Yazami, R.; Touzain, Ph. *J. Power Sources* **1983**, *9*, 365.
(4) Dahn, J. R.; Sleigh, A.; Shi, H.; Way, B.; Weydanz, W.; Reimer, J. N.; Zhong, Q.; Von Sackhen, U. In *Lithium Batteries−New Materials, Development and Perspectives*; Pistoia, G., Ed.; Elsevier: Amsterdam, 1994.
(5) Dahn, J. R.; Zhen, T.; Liu, Y.; Xue, J. S. *Science* **1995**, *270*, 590.
(6) Nishijima, M.; Tadokoro, N.; Takeda, Y.; Imanishi, N.; Yamamoto, O. *J. Electrochem. Soc.* **1994**, *141*, 2966.
(7) Nishijima, M.; Kagohashi, T.; Takeda, Y.; Imanishi, M.; Yamamoto, O. *J. Power Sources* **1997**, *68*, 510.
(8) Shodai, T.; Okada, S.; Tobishima, S.; Yamaki, J. *J. Power Sources* **1997**, *68*, 515.
(9) Shodai, T.; Sakurai, Y.; Suzuki, T. *Solid State Ionics* **1999**, *122*, 85.
(10) James, A. C. W. P.; Ellis, B.; Goodenough, J. B. *Solid State Ionics* **1988**, *27*, 45.
(11) Lavela, P.; Pérez Vicente, C.; Tirado, J. L.; Branci, C.; Olivier-Fourcade, J.; Jumas, J. C. *Chem. Mater.* **1999**, *11*, 2687.
(12) Dedryvère, R.; Denis, S.; Pérez Vicente, C.; Olivier-Fourcade, J.; Jumas, J. C. *Chem. Mater.*, in press.
(13) Murphy, D. W.; DiSalvo, F. J.; Carides, J. N.; Waszczak, J. V. *Mater. Res. Bull.* **1978**, *13*, 1395.
(14) Courtney, I. A.; Dahn, J. R. *J. Electrochem. Soc.* **1997**, *144* (6), 2045.
(15) Denis, S.; Baudrin, E.; Touboul, M.; Tarascon, J. M. *J. Electrochem. Soc.* **1997**, *144* (12), 4099.
(16) Denis, S.; Baudrin, E.; Orsini, F.; Ouvrard, G.; Touboul, M.; Tarascon, J. M. *J. Power Sources* **1999**, *81-82*, 79.

10.1021/cm001084d CCC: $19.00
Published on Web 11/22/2000

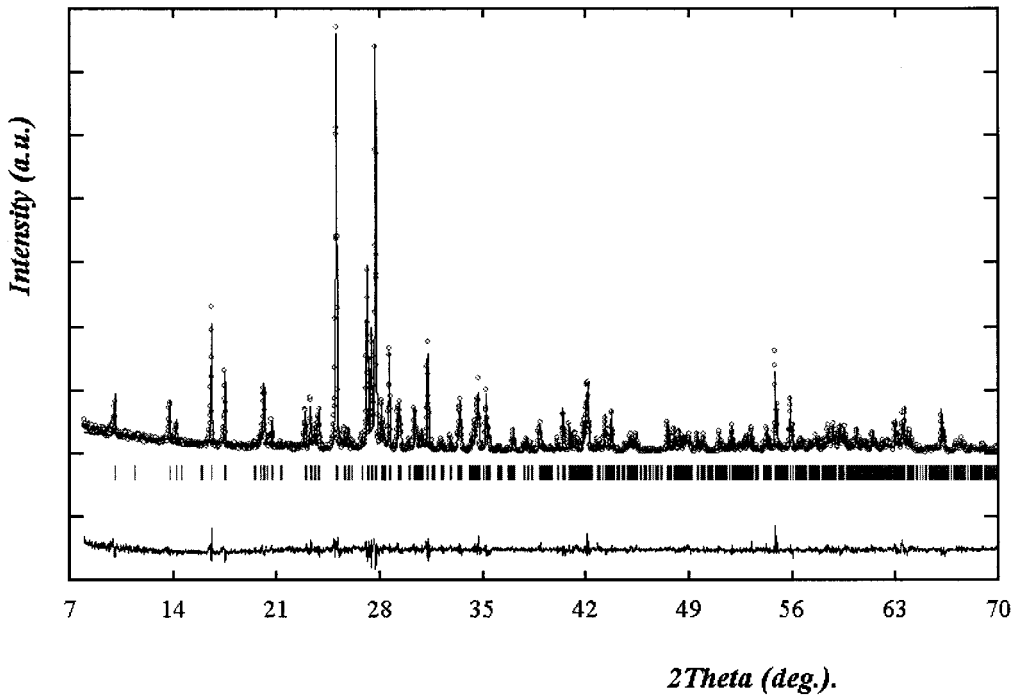

Figure 1. X-ray diffraction pattern ($\lambda_{CuK\alpha}$ = 1.5418 Å) and Rietveld refinement of triclinic $FeVO_4$. The upper traces represent the observed (points) and calculated (solid line) XRD patterns while the lower trace is a plot of the difference (observed minus calculated). The vertical marks show the positions calculated for Bragg reflections.

the basis of these results, a Li-reaction mechanism different from the classical insertion/deinsertion process had been proposed to explain the great acceptance of lithium ions within vanadates.[15]

To propose a definitive mechanism, a complementary ^{57}Fe Mössbauer study has been undertaken at different discharge and charge steps of an $FeVO_4$/Li battery and is reported in the present paper.

2. Experimental Section

2.1. Synthesis. A 20-g sample of triclinic $FeVO_4$ was obtained by annealing the amorphous precursor $FeVO_4 \cdot 2.7H_2O$ at 700 °C during 15 h under air flow. The latter was synthesized by a soft chemistry process using ammonium metavanadate NH_4VO_3 (Prolabo) and iron nitrate $Fe(NO_3)_3 \cdot 9H_2O$ (Aldrich) as starting materials. Stoichiometric amounts of both compounds were separately dissolved in aqueous media in order to prepare 4.3×10^{-2} and 0.26 mol·L^{-1} solutions, respectively. The synthesis method consisted in slowly adding the iron-based solution to the ammonium metavanadate one in order to obtain a homogeneous precipitate and keep a pH value close to ~2.5. Simultaneously, the mixture was stirred and heated at 50 °C. We experienced that the slow addition is a critical parameter to the phase purity especially when preparing such large amounts, since it directly influences the pH value. Then, the precipitate was first dissolved by decreasing the pH value to 1 using a nitric acid solution (6 mol·L^{-1} HNO_3) and second raised to ~4 by gently adding an ammoniacal solution (6 mol·L^{-1} NH_4OH). Finally, the precipitate was recovered by centrifugation, washed several times with water and acetone, and dried overnight at 50 °C.

The Fe/V ratio was checked with an EDS analyzer (Link Oxford). X-ray powder diffraction measurements, recorded by means of a Philips diffractometer (PW1710) using Cu Kα radiation (λ = 1.5418 Å), were performed on the annealed material and confirmed triclinic $FeVO_4$ as a single phase (as shown in Figure 1). Rietveld refinement of this XRD pattern was carried out with the program FULLPROF 98[17] derived from the Rietveld version DBW3.2S(8804)[18] and running on a PC computer under Windows 95. The structural parameters were in good agreement with the results reported by Robertson and Kostiner.[19]

2.2. Electrochemical Measurements. Swagelok test cells were built using triclinic $FeVO_4$ as the active positive electrode material and Li metal as the active negative electrode material, both separated by a glass fiber separator soaked in a 1 M $LiPF_6$ in EC/DMC (2:1 weight ratio) electrolyte solution. The plastic positive electrode was elaborated using Bellcore's PLiON technology, which consists in mixing 7% super P carbon black (SP), 53% of the active material, 16% PVDF−HFP copolymer, and 24% dibutyl phthalate (DBP) in acetone. The resulting intimately mixed paste was then deposited on a glass plate to produce, after acetone evaporation, the positive laminate from which 1 cm^2 disks were cut. Prior to being used as the positive electrode in Swagelok cells, the disks were immersed in diethyl ether to remove the DBP plasticizer. The Swagelok test cells were then assembled in a glovebox filled with argon gas. Electrochemical measurements were carried out by means of a "Mac-Pile" system (Biologic, Claix, France) operating in a galvanostatic mode.

For Mössbauer studies, the cells were cycled at a current rate of 1 Li in 40 h (corresponding to a current density close to 0.3 mA/cm^2) until a fixed composition of Li_xFeVO_4 was achieved. Li_xFeVO_4 absorbers of approximately 120 mg/cm^2 (active material weight) were heat-sealed under argon flow in metallized plastic bags, prior to being studied by Mössbauer spectroscopy.

2.3. Mössbauer Measurements. ^{57}Fe Mössbauer spectra were collected at room temperature on a EG&G spectrometer operating in the constant-acceleration mode with a ^{57}Co(Rh) source. The velocity scale was calibrated by using the magnetic sextet spectrum of a metallic iron foil absorber. Recorded

(17) Rodriguez-Carjaval, J. *FULLPROF*: *A Program for Rietveld Refinement and Pattern Matching Analysis*. Abstracts of the Satellite Meeting on Powder Diffraction of the XV Congress of the IUCr, Toulouse, France, 1990; p 127.

(18) Wiles, D. B.; Sakthivel, A.; Young, R. A. In *User's Guide to Program DBW3.2S* (version 8804); Georgia Institute of Technology, Atlanta, 1988.

(19) Robertson, R.; Kostiner, E. *J. Solid State Chem.* **1972**, *4*, 29.

Table 1. Hyperfine Parameters of Refined ^{57}Fe Mössbauer Spectra of Triclinic $FeVO_4$ and Lithiated Li_xFeVO_4 Obtained in the Discharged State[a]

sample ref	x in Li_xFeVO_4	site[b]	δ_{IS} ($mm\cdot s^{-1}$)	Δ_{QS} ($mm\cdot s^{-1}$)	RA (%)	Γ_{LW}[c] ($mm\cdot s^{-1}$)	absorption (%)
A	0	Fe^{III} Tbp	0.314(3)	1.097(6)	34.4	0.26	7.28
		Fe^{III} Octa	0.379(4)	0.591(7)	33.6		
		Fe^{III} Octa	0.394(3)	0.239(1)	31.9		
B	0.2	Fe^{III} Tbp	0.36(1)	1.12(1)	23.4	0.31	9.4
		Fe^{III} Octa	0.41(1)	0.62(1)	35.8		
		Fe^{III}Octa	0.40(1)	0.25(1)	33.5		
		Fe^{II}	1.47(4)	0.74(7)	3.1		
		Fe^{II}	1.41(3)	0.32(4)	4.1		
C	0.5	Fe^{III} Tbp	0.38(5)	0.91(8)	7.9	0.38	8.33
		Fe^{III} Octa	0.40(1)	0.57(2)	33.2		
		Fe^{III} Octa	0.36(1)	0.17(2)	26.4		
		Fe^{II}	1.38(2)	0.76(3)	16.1		
		Fe^{II}	1.39(2)	0.31(2)	16.4		
D	1	Fe^{0} Cov	0.16(1)	0.14(3)	23.2	0.44	6.07
		Fe^{III}	0.29(2)	0.93(4)	29.0		
		Fe^{III}	0.30(4)	0.60(8)	14.6		
		Fe^{II}	1.37(1)	0.60(2)	14.2		
		Fe^{II}	1.46(1)	1.12(2)	19.0		
E	2	Fe^{0} Cov	−0.04(3)	0.38(3)	10.2	0.37	5.54
		Fe^{III}	0.41(1)	0.85(2)	32.1		
		Fe^{III}	0.43(1)	0.32(1)	29.9		
		Fe^{II}	1.49(2)	0.27(2)	13.4		
		Fe^{II}	1.51(2)	0.84(3)	14.4		
F	3	Fe^{0} Cov	−0.02(2)	0.36(3)	13.8	0.40	7.61
		Fe^{III}	0.44(1)	0.75(2)	28.5		
		Fe^{III}	0.46(1)	0.26(1)	31.0		
		Fe^{II}	1.39(2)	0.28(2)	15.8		
		Fe^{II}	1.42(2)	0.76(4)	10.8		
G	4	Fe^{0} Cov	0.03(2)	0.38(3)	16.2	0.45	8.85
		Fe^{0} Cov	0.14(2)	1.04(2)	26.8		
		Fe^{0} Cov	0.22(2)	0.31(2)	28.9		
		Fe^{II}	1.12(2)	0.33(2)	14.0		
		Fe^{II}	1.23(1)	0.84(2)	14.1		
H	5	Fe^{0} Cov	0.13(1)	0.24(1)	34.1	0.42	8.2
		Fe^{0} Cov	0.16(1)	1.28(2)	22.1		
		Fe^{0} Cov	0.14(1)	0.85(2)	29.3		
		Fe^{II}	1.32(2)	0.33(3)	9.9		
		Fe^{II}	1.34(5)	0.80(8)	4.6		
I	6	Fe^{0} Cov	−0.09(1)	0.84(2)	24.8	0.42	11.15
		Fe^{0} Cov	−0.070(6)	0.263(9)	39.9		
		Fe^{0} Cov	0.10(1)	1.05(2)	25.8		
		Fe^{II}	1.15(3)	0.54(4)	5.5		
		Fe^{II}	1.45(3)	0.87(5)	4.0		
J	7	Fe^{0} Cov	−0.117(4)	0.264(7)	47.7	0.43	10.6
		Fe^{0} Cov	−0.111(9)	0.79(1)	29.4		
		Fe^{0} Cov	0.106(9)	1.06(2)	22.9		
K	8	Fe^{0} Cov	−0.179(8)	0.22(2)	42.8	0.378	13.5
		Fe^{0} Cov	−0.17(1)	0.59(2)	42.0		
		Fe^{0} Cov	−0.09(2)	1.00(3)	15.2		

[a] δ_{IS} = isomer shift, Δ_{QS} = quadrupole splitting, Γ_{LW} = full width at half-maximum, RA (%) = relative area. [b] Tbp = Trigonal bipyramid, Octa = Octahedra, Cov = covalent. [c] Γ_{LW} values were constrained to be equal for all components.

spectra were fitted to Lorentzian profiles by a least-squares method,[20] and the fit quality was controlled by the classical χ^2 test. All isomer shifts reported in this paper are given with respect to the center of the α-Fe spectrum recorded at room temperature with the same source.

3. ^{57}Fe Mössbauer Results

3.1. Triclinic $FeVO_4$. The ^{57}Fe Mössbauer spectrum of triclinic $FeVO_4$ (Figure 2) can be fitted with three quadrupole-split doublets of equal intensity, with the following isomeric shifts: $\delta_{IS} = 0.314$, 0.379, and 0.394 $mm\cdot s^{-1}$ (Table 1), which are characteristic of Fe^{III} in an

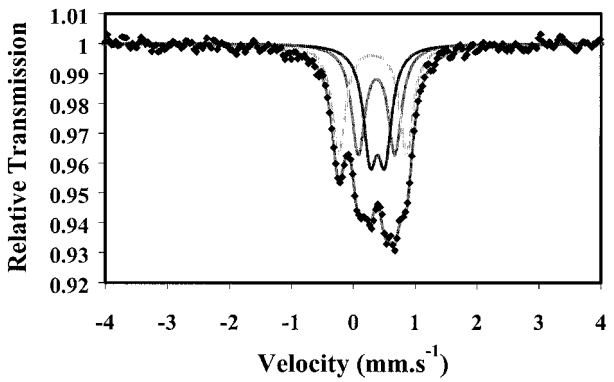

Figure 2. ^{57}Fe Mössbauer spectra of triclinic $FeVO_4$, collected at room temperature.

(20) Kündig, W. *Nucl. Instrum. Methods* **1969**, *75*, 336.

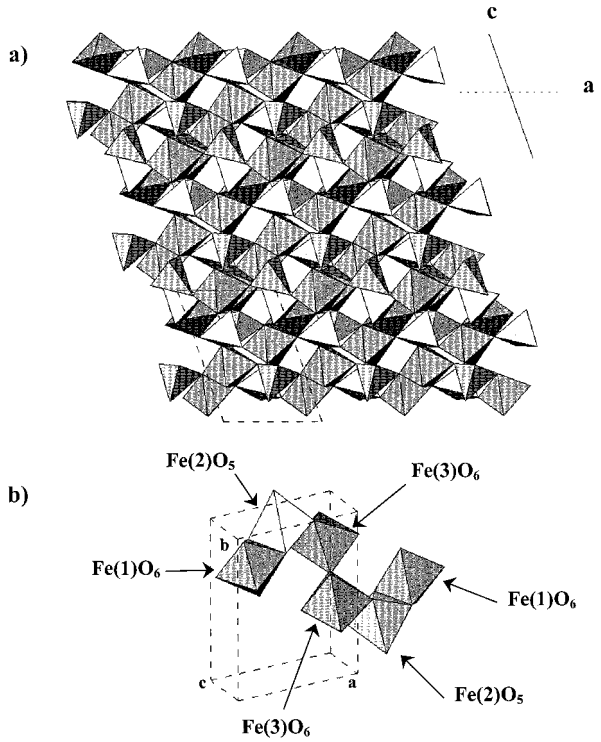

Figure 3. (a) Structure of triclinic $FeVO_4$. (b) Projection of a double bent chains on the (001) plane.

oxygenated environment.[21] The corresponding quadrupole splitting values are $\Delta_{QS} = 1.097$, 0.591, and 0.239 mm·s^{-1}, respectively, and each signal can be attributed to a particular iron site. These results are consistent with the $FeVO_4$ structure illustrated in Figure 3. As previously reported in the literature,[19] iron atoms are equally distributed in three different sites: two FeO_6 distorted octahedra (leading to the lowest quadrupole splittings) and one FeO_5 distorted trigonal bipyramid (denoted Tbp in Table 1) leading to the greatest quadrupole splitting. The decrease in the Mössbauer isomeric shift is consistent with the decrease in the coordination number of iron atoms. As a three-dimensional view, the structure consists of double bent chains of edge-sharing FeO_6 octahedra and FeO_5 trigonal bipyramids, linked together by VO_4 tetrahedra.

3.2. Lithiated Materials Li_xFeVO_4. Figure 4 represents the voltage−composition profiles of a triclinic $FeVO_4$/Li cell during the first discharge−charge cycle within two potential ranges: 0.02 V/3.5 V and 0.4 V/2 V. The marks, labeled from A to M, correspond to different Li_xFeVO_4 compositions studied by ^{57}Fe Mössbauer spectroscopy.

3.2.1. Discharged Samples (from A to K). On Figure 5 are displayed the ^{57}Fe Mössbauer spectra of the Li_xFeVO_4 samples obtained during the first discharge. The refined hyperfine parameters are reported in Table 1.

Dramatic modifications are observed at the beginning of the lithium reaction. Five subspectra are needed to fit correctly the $x = 0.2$ and $x = 0.5$ Mössbauer spectra (samples B and C) compared to three needed for the initial compound ($x = 0$, sample A, Figure 1). Three contributions can be ascribed to Fe^{III} ($0.3 < \delta_{IS}$/mm·s^{-1} < 0.4) with almost the same symmetry characteristics as previously mentioned (i.e., two Fe^{III} and one Fe^{III} sites in octahedral and trigonal bipyramid environments, respectively). However, this first reduction step seems to specifically affect Fe^{III} in the trigonal bipyramid site since its contribution to the Mössbauer spectrum drops from 34% to 23% and then down to 8% for the $x = 0.2$ and $x = 0.5$ samples, respectively. In addition, two new quadrupole-split doublets occurring in the range 1.4−1.5 mm·s^{-1} indicate the appearance of two sites of Fe^{II} in the oxygenated environment. Their relative contribution increases up to 32% in total, while the component corresponding to one of the octahedrally coordinated Fe^{III} site is slightly affected (its relative area decreases from 33% to 26%). So we can assume that an $Fe^{III} \rightarrow Fe^{II}$ reduction occurs at the beginning of lithium introduction in triclinic $FeVO_4$ and seems to take place first on the trigonal bipyramid site and then on one of the 6-fold coordinated Fe^{III} site. This iron reduction step should be at the origin of the two-phase reaction previously shown by in situ XRD measurement when $0 < x < 0.625$.[16]

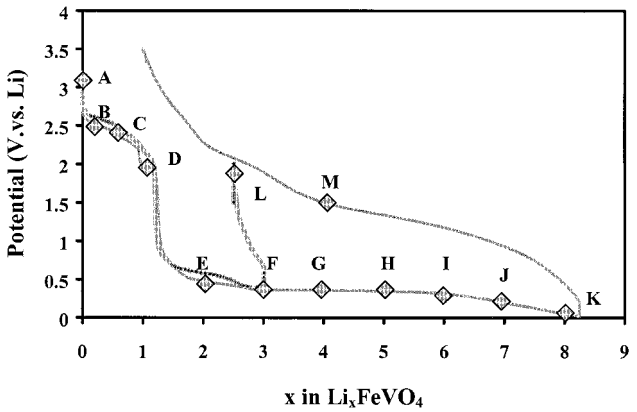

Figure 4. Discharge−charge profile of a triclinic $FeVO_4$/Li cell.

For $0.5 < x < 2$ (spectra D and E), no important variation of the refined hyperfine parameters is noted regarding the Fe^{III} and Fe^{II} sites, although their total relative contributions to the spectrum are slightly reduced to 62% and 27%, respectively. At this stage, spectra can be fitted considering two Fe^{III} and two Fe^{II} subspectra. In addition, a significant decrease in the isomer shift value is observed for one subspectrum ($\delta_{IS} = 0.16$ and -0.04 mm·s^{-1} for $x = 1$ and $x = 2$, respectively). This evolution can be attributed to an increase in the covalent character of the Fe−O bonding. *Therefore, this subspectrum has been assigned to covalent iron.* This *evolution* implies a structure modification and/or the appearance of a multiphase system. Note that the first hypothesis would be consistent with the in situ XRD results, which demonstrate the formation of a cubic phase ($a = 4.16$ Å, $Fm3m$).[16]

For $2 < x < 4$ (spectra F and G), *the whole spectrum is overall shifted to the low isomer shifts, indicating an increase in the covalent character of the Fe−O bonds. Thus, the total area of the components ascribed to covalent Fe increases up to 72%. This could be at the origin of the structural breakdown which starts to take place at $x = 3.75$ according to the in situ XRD measurements.*

For $x = 5$ (sample H), *the contributions of the Fe^{II} sites decrease to 14% together with the increase in the amount*

(21) Mesnil, F. *J. Phys. Chem. Solids* **1985**, *46* (7), 763.

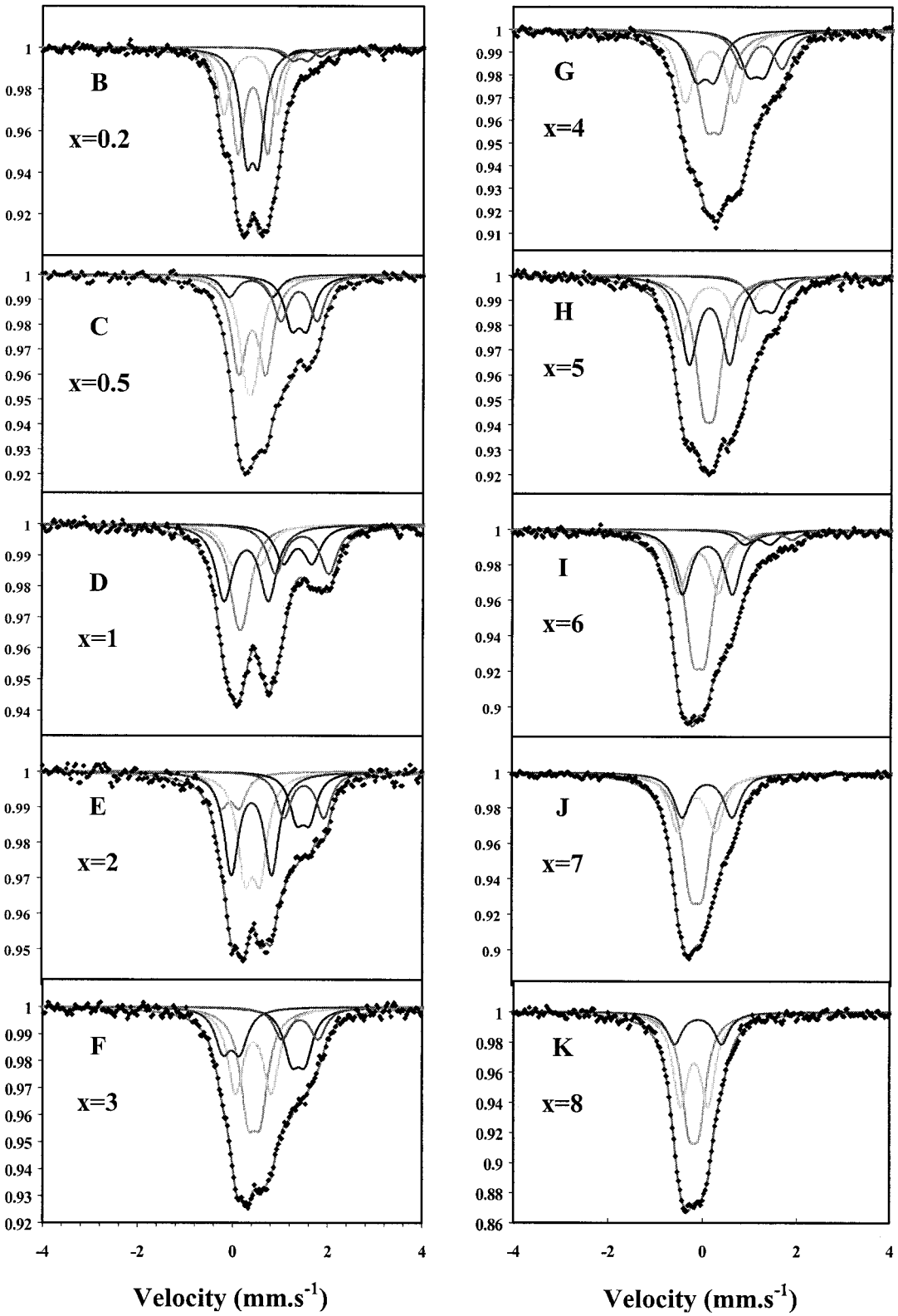

Figure 5. Room temperature ^{57}Fe Mössbauer spectra of lithiated Li_xFeVO_4 obtained at different discharged states.

of covalent Fe. Upon further discharging the cell, $x > 6$ (samples J and K), the Fe^{II} contributions vanish as well, so that the Mössbauer spectra (for $x = 7$ and 8) can be fitted with only three components, all ascribed to *covalent* Fe^0. All these modifications give evidence of a complex and simultaneous reduction: $Fe^{III} \rightarrow Fe^{II} \rightarrow Fe^0$ or $Fe^{III} \rightarrow Fe^{II}$, Fe^0.

3.2.2. Charged Samples. Two samples have been studied by ^{57}Fe Mössbauer spectroscopy: $Li_{2.5}FeVO_4$ (sample L) and $Li_{4.0}FeVO_4$ (sample M). The Mössbauer spectra are reported in Figure 6, and the refined hyperfine parameters are listed in Table 2.

Sample L: *$Li_{2.5}FeVO_4$*. This sample corresponds to the discharge of an $FeVO_4$/Li cell to 0.4 V (leading to the insertion of 3 Li/mol) followed by its recharge up to 2 V. This second step is not much reversible as only 0.5 Li/mol can be removed (Figure 4). The Mössbauer spectrum (Figure 6a) is very similar to the one obtained

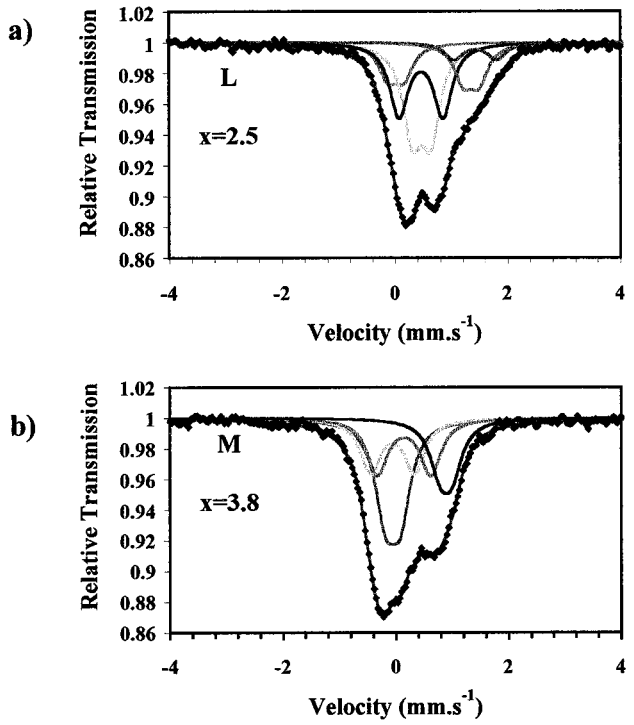

Figure 6. Room temperature ^{57}Fe Mössbauer spectra of lithiated Li_xFeVO_4 obtained at two different charged states.

for $Li_{3.0}FeVO_4$ (sample F). The main difference concerns the relative areas of the Fe^{II} and Fe^{III} contributions, which indicate a selective oxidation of Fe^{II} into Fe^{III} while the *covalent Fe* sites are not affected upon this charge step. This result gives evidence of the irreversible character of the recharge: it is not possible to get back the initial structure once *covalent Fe* is formed.

Sample M: *$Li_{3.8}FeVO_4$*. For this sample, which is amorphous to the X-ray, an $FeVO_4$/Li cell has been discharged down to 0.02 V (like for sample K, $Li_{8.0}FeVO_4$) and then recharged to 1.5 V. The Mössbauer spectrum (Figure 6b) is very similar to the ones obtained at 6−7 Li/mol in the discharge, concerning the three Fe^0 components. An additional contribution, for which $\delta_{IS} = 0.9$ mm·s^{-1}, is needed to fit correctly the experimental data and can be ascribed to Fe^{II}. So, at this point, thanks to Mössbauer spectroscopy, we have evidence of Fe^0 occurrence during the Li uptake and its reoxidation into Fe^{II} upon the following charge to 1.5 V. On the other hand, this spectrum is completely different from the one recorded for sample G ($Li_{4.0}FeVO_4$ obtained at 0.35 V during the first discharge). This observation indicates that the structural modifications involved upon the lithium uptake are completely irreversible and are in good agreement with the XRD data.

4. Discussion

Since ^{57}Fe Mössbauer spectroscopy is sensitive to the local electronic properties around the iron sites in a material, this technique allows information on the iron oxidation state and its symmetry site throughout the Li introduction in triclinic $FeVO_4$. The most important results gathered during this study are the following:

(i) A $Fe^{III} \rightarrow Fe^{II}$ reduction step occurs specifically on the trigonal bipyramid sites at the beginning of the lithium uptake.

(ii) *Covalent Fe appears as soon as one lithium ion* has reacted with $FeVO_4$, and its amount progressively increases with the lithium introduction.

(iii) A complex and simultaneous reduction process $Fe^{III} \rightarrow Fe^{II} \rightarrow Fe^0$ or $Fe^{III} \rightarrow Fe^{II}$, Fe^0 has been demonstrated during the first discharge.

Now we are going to combine these ^{57}Fe Mössbauer results with the ones previously obtained by XRD and XANES measurements recorded at both V and Fe K edges,[16] in order to get a better insight into the lithium reaction mechanism with vanadates.

At the beginning of the discharge of a triclinic $FeVO_4$/Li cell ($0 < x < 1.125$), both Fe^{III} and V^V are partially reduced to Fe^{II} and V^{IV}, respectively, leading to a phase transformation followed by a solid solution as shown by XRD measurements. As the Mössbauer data reveal that the $Fe^{III} \rightarrow Fe^{II}$ reduction takes place specifically on the trigonal bipyramid sites as soon as 0.2 Li is introduced in $FeVO_4$, we can believe that this reduction step is at the origin of the first phenomenon, i.e., the phase transformation. Afterward the progressive disorganization of this structure, as shown by XRD measurements, is consistent with the increase in the covalent character of the Fe−O bonding obtained from Mössbauer spectroscopy. The $1.125 < x < 2.75$ composition range corresponds to the formation of a new cubic $LiFeO_2$-type phase, for which the following formula can be proposed: $Li_xFe^{III}_{1-y}Fe^{II}_yV_zIVO_4$. *In the meantime, Mössbauer spectroscopy indicates the presence of covalent iron, which induces the appearance of a phase decomposition.* Then, for $2.75 < x < 3.75$, V^{IV} is reduced to V^{III}, which can explain the a solid solution of the previous cubic phase. Finally, until the end of the discharge, *covalent Fe^0 appears and its amount continuously increases* to the detriment of the solid solution, which tends to be consumed. After the reaction of 6 Li ions, an amorphous material containing Fe^0 and V (whose oxidation state is about +2) is obtained and remains until the end of the discharge. The XANES results for both Fe and V K edges also indicate that the electronic states are completely delocalized, which is in good agreement with the formation of an amorphous material.

At the end of the charge (up to 3.5 V, corresponding to the composition $Li_{1.0}FeVO_4$), the material is still amorphous. XANES data indicate that the oxidation states of iron and vanadium are almost 2.7 and 4, respectively. Although the sample studied by Mössbauer spectroscopy is only recharged up to 1.5 V, this reoxidation step has been confirmed concerning the iron atoms by a partial oxidation of Fe^0 into Fe^{II}.

As eight lithium ions react with triclinic $FeVO_4$ upon the first discharge of the battery, we can simply consider the reduction of Fe^{III} and V^V to the metallic elements mixed in a Li_2O matrix. However, this reaction is difficult to conceive since both vanadium and iron atoms are reoxidized during the following charge of the battery. In addition, the possibility of an alloy formation (like, e.g., in the Li−Sn system[14]) is also excluded because none exists in the Li−Fe and Li−V systems. Therefore, in light of these considerations, we may wonder if the three contributions to the Mössbauer spectra, evidenced at the end of the discharge and ascribed to Fe^0 sites, are really characteristic of the

Table 2. Hyperfine Parameters of Refined ^{57}Fe Mössbauer Spectra of Lithiated Li_xFeVO_4 Obtained in the Charged State[a]

sample ref	x in Li_xFeVO_4	site	δ_{IS} ($mm \cdot s^{-1}$)	Δ_{QS} ($mm \cdot s^{-1}$)	RA (%)	Γ_{LW}[c] ($mm \cdot s^{-1}$)	absorption (%)
L	2.5	Fe^0 Cov	0.02(2)	0.29(2)	13.1	0.40	12.1
		Fe^{III}	0.48(1)	0.32(1)	35.6		
		Fe^{III}	0.46(1)	0.78(2)	29.8		
		Fe^{II}	1.36(2)	0.28(2)	14.5		
		Fe^{II}	1.43(3)	0.76(5)	7.0		
M	3.8	Fe^0 Cov	−0.05(2)	0.26(1)	35.6	0.44	13.3
		Fe^0 Cov	−0.06(2)	0.78(3)	22.0		
		Fe^0 Cov	0.15(2)	0.95(3)	23.2		
		Fe^{II}	0.89(2)	0.20(3)	19.3		

[a] δ_{IS} = isomer shift, Δ_{QS} = quadrupole splitting, Γ_{LW} = full width at half-maximum, RA (%) = relative area. [b] Cov = covalent. [c] Γ_{LW} values were constrained to be equal for all components.

presence of metallic iron or not. First, if it was true, the Mössbauer spectrum should consist of magnetic sextuplets. However, as reported on Fe_2O_3[22] or $TaFe_{1.25}Te_3$[23,24] samples, the particle size can play an important role, reducing the sextuplet to a doublet when the material is finely divided, which is our case since our material is getting amorphous. The result that allows us to give an answer is the possibility of oxidizing Fe^0 upon the lithium removal of the Li_xFeVO_4/Li cell. This clearly indicates that these iron atoms are still in interaction with the oxygen atoms in the amorphous matrix, constituting a very covalent phase. This increase in the covalency is also in good agreement with the XANES results characteristic of delocalized electronic states.[16]

So how can we explain this behavior? We can refer to the two-step mechanism we previously proposed,[15,16] which was the following: (i) a decomposition process occurs during the first lithium uptake leading to a mixture of an inert matrix Li-M−O and an electrochemically active Li−V−O phase and (ii) the oxygen is acting as a redox center leading to possible "Li−O" interactions thereby leading to the enhanced observed capacity. In the present case, both Fe and V seem to be involved in the electrochemically active matrix. On the other hand, vanadates are not the only materials, for which the anion plays an important role during lithium reaction. For example, this behavior was already pointed out during the XANES study on TiS_2[25] or by the computational work done on $LiMO_2$ materials (M = Co, Ni, V, etc.).[26] More recently, ^7Li NMR and XAS studies performed on molybdenum oxides[27] also evidenced the formation of Li−O interactions. In the same way, the Mössbauer study performed on tin oxide, SnO, upon lithium insertion is another example.[28] Finally, we can quote the work done on nitrides by Shodai et al.,[9] who showed that cobalt oxidation in $Li_{2.6}Co_{0.4}N$ could not totally explain the extraction of 1.6 Li/mol, so that the role of the anion should be taken into account. This way, they studied the charge distributions of $Li_{2.6}Co_{0.4}N$ and the electrochemically oxidized $Li_{1.0}Co_{0.4}N$ sample by using core-level electron energy loss spectroscopy (EELS).[29] These measurements indicated that the occupancy of the nitrogen 2p orbitals was reduced by the lithium extraction (from $Li_{2.6}Co_{0.4}N$ to $Li_{1.0}Co_{0.4}N$) and that there was a large quantity of holes in these orbitals. The author also reported that cobalt and nitrogen covalency gradually strengthened when lithium ions were extracted. So they concluded by proposing a reaction mechanism where both cobalt and nitrogen play an important role in maintaining the charge balance. This is another example emphasizing the anion role during lithium reaction.

Coming back to vanadates, we are now able to propose a mechanism based on lithium "adsorption" leading to Fe−"O−Li" and V−"O−Li" interactions. Since the electrochemical reduction leads to a finely divided material, we can consider that the surface particles become highly reactive especially at the nanometric scale. In that case, lithium ions could be "adsorbed" in such a manner that the electrons would be injected in the conduction band of the material leading to delocalized electronic states and a reinforcement of the Fe−O and V−O covalent character, which is perfectly consistent with the XANES and Mössbauer results. This would explain why the material seems to behave like a metal whereas it is in strong interaction with the oxygen matrix.

5. Conclusion

A ^{57}Fe Mössbauer study allowed us to give additional information on the mechanism occurring upon the lithium reaction with triclinic $FeVO_4$, compared to the XANES and XRD measurements previous. The beginning of this reaction seems to correspond to a classical insertion process with an $Fe^{III} \rightarrow Fe^{II}$ reduction, which specifically affects the trigonal bipyramid sites, and leads to a phase transformation. *Evidence of Fe^0 has been shown at the end of the discharge, leading to an irreversible structural breakdown.* To take into account the reoxidation of both iron and vanadium upon the next charge of the battery, the previously proposed mechanism, consisting in the formation of "Li−O" interactions, has been slightly modified and is now based on lithium adsorption on the particles surface of the obtained nanomaterial.

CM001084D

(22) Kündig, W.; Bömmel, H.; Constabaris, G.; Lindquist, R. H. *Phys. Rev.* **1966**, *142*, 327.
(23) Badding, M. E.; Li, J.; DiSalvo, F. J.; Zhou, W.; Edwards, P. P. *J. Solid State Chem.* **1992**, *100*, 313.
(24) Pérez Vicente, C.; Womes, M.; Jumas, J. C.; Sanchez, L.; Tirado, J. L. *J. Phys. Chem. B* **1998**, *102*, 8712.
(25) Wu, D. Y.; Ouvrard, G.; Lemaux, S.; Moreau, P.; Gressier, P.; Lemoigneau, F.; Rouxel, J. *Phys. Rev. Lett.* **1996**, *77*, 2101.
(26) Ceder, G.; Aydinol, M. K.; Kohan, A. F. *Comput. Mater. Sci.* **1997**, *8*, 161.
(27) Leroux, F.; Goward, G. R.; Power, W. P.; Nazar, L. F. *Electrochem. Solid State Lett.* **1998**, *1*, 255.
(28) Chouvin, J.; Olivier-Fourcade, J.; Jumas, J. C.; Simon, B.; Godiveau, O. *Chem. Phys. Lett.* **1999**, *308*, 413.
(29) Suzuki, S.; Shodai, T.; Yamaki, J. *J. Phys. Chem. Solids* **1998**, *59*, 331.